Substitution pattern on anthrol carbaldehydes: excited state intramolecular proton transfer (ESIPT) with a lack of phototautomer fluorescence

S. Chaiwongwattana, D. Skalamera, N. Doslic, C. Bohne & N. Basaric

October 2017

The final publication is available via Royal Society of Chemistry at:

https://doi.org/10.1039/C7CP05472F

Journal Name

ARTICLE

Substitution Pattern on Anthrol Carbaldehydes: Excited State Intramolecular Proton Transfer (ESIPT) with a Lack of Phototautomer Fluorescence

Received 00th January 20xx,
Accepted 00th January 20xx

DOI: 10.1039/x0xx00000x

www.rsc.org/

S. Chaiwongwattana,[a] Đ. Škalamera,[b] N. Došlić,[c]* C. Bohne[d] and N. Basarić[b]*

Photophysical properties and excited state intramolecular proton transfer (ESIPT) reactivity for anthrol carbaldehydes **1**-**5** have been investigated computationally and experimentally by steady-state and time-resolved fluorescence and laser flash photolysis (LFP). 1,2-Disubstituted anthrol carbaldehydes **1** and **2** are not ESIPT reactive, contrary to naphthol analogues. The main deactivation channels from S_1 for **1** and **2** are fluorescence (Φ_F = 0.1-0.2) and intersystem crossing (ISC) to almost isoenergetic T_2 states. The triplet states from **1** and **2** were detected by LFP (in N_2-purged CH_3CN, τ = 15 ± 2 μs for **1**, and τ = 5.5 ± 0.1 μs for **2**). In contrast, 2,3-disubstituted anthrols **3**-**5** undergo efficient barrierless ultrafast ESIPT. However, the typical dual emission from locally excited states and ESIPT tautomers were not observed since ESIPT proceeds *via* a conical intersection with S_0 delivering the keto-tautomer in the hot ground state. Therefore, anthrols **3**-**5** are about ten times less fluorescent compared to **1** and **2**, and the emission for **3**-**5** originates from less-populated conformers that cannot undergo ESIPT. Keto-tautomers for **3**-**5** were detected in CH_3CN by LFP (λ_{max} = 370 nm, τ = 30-40 ns). The difference in ESIPT reactivity for **1**-**3** was fully disclosed by calculations at ADC(2)/aug-cc-pVDZ level of theory, and particularly, by calculation of charge redistribution upon excitation to S_1. Only 2,3-disubstituted anthrols exhibit polarization in S_1 that increases the electron density on the carbonyl and decreases this density on the phenolic OH, setting the stage for ultrafast ESIPT.

Introduction

Some organic chromophores exhibit enhanced acidity or basicity upon electronic excitation.[1,2] If acidic and basic sites are in close proximity, excitation can lead to excited-state intramolecular proton transfer (ESIPT).[3,4] ESIPT has been intensively investigated over five decades because of its fundamental aspect in chemistry and biology.[5] Furthermore, ESIPT found numerous applications, primarily in material science,[6,7] but also in the fields of sensing,[8-13] bioimaging,[14-16] solar energy conversion,[17] UV-photostabilizers,[18-22] laser dyes,[23-27] organic light-emitting devices,[28,29] long-lived pH jumps,[30] molecular switches,[31,32] or switching of polymorphs.[33] The most common acidic group in ESIPT reactions is phenolic OH,[34] whereas the basic site is usually encountered in a carbonyl group,[35] or a nitrogen atom in a heterocycle.[36] The first molecule that was experimentally found to undergo ESIPT was salicylic acid.[37] Later, salicylaldehyde derivatives were studied[38,39] and the ESIPT was investigated theoretically.[40] The reaction scope was extended to naphthol carbaldehyde derivatives.[41-44] Extending the size of chromophore has advantages because larger molecules can be excited by near-visible light available from the usual laser sources, and emission in the visible spectrum enables applications in different aspects of sensing and material science. We investigated how the increase of the size from naphthalene to anthracene affects the photophysics and ESIPT reactivity of these larger molecules. The known differences in the photophysics of naphthalene and anthracene chromophores makes predictions as to the ESIPT reactivity of anthrol carbaldehydes not possible a priori. The key differences between the naphthalene and anthracene photophysics are in the ordering of the singlet and triplet excited states energy levels, where competitive pathways such as intersystem crossing (ISC) are expected to play a more important role for anthracenes. Moreover, anthracenes ESIPT reactivity could also be significantly affected by the different position of the energy levels imposed by different substitution patterns.[45] Herein we report the investigation of the photophysical

[a] *Institute of Science, Suranaree University of Technology, 30000 Nakhon Ratchasima, Thailand.*
[b] *Department of Organic Chemistry and Biochemistry, Ruđer Bošković Institute, Bijenička cesta 54, 10 000 Zagreb, Croatia. Fax: + 385 1 4680 195; E-mail: nbasaric@irb.hr.*
[c] *Department of Physical Chemistry, Ruđer Bošković Institute, Bijenička cesta 54, 10000 Zagreb, Croatia. Fax: + 385 1 4680 245; E-mail: nadja.doslic@irb.hr.*
[d] *Department of Chemistry, University of Victoria, Box 1700 STN CSC, Victoria BC, V8W 2Y2, Canada.*

† Electronic Supplementary Information (ESI) available: Calculation data for **1**-**3**, UV-vis and fluorescence spectra of **1**-**5**, LFP data and ^1H and ^{13}C NMR spectra. This material is available free of charge via the Internet. See DOI: 10.1039/x0xx00000x

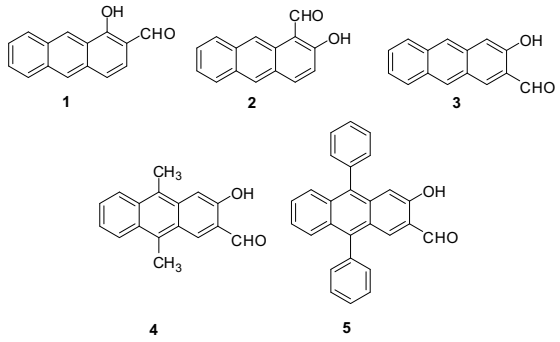

Fig. 1. Anthrol carbaldehydes **1**-**5**. Synthesis of the molecules is described in literature precedent[46,47] and in the ESI (Schemes S1-S3).

properties and ESIPT reactivity for a series of anthrol carbaldehydes **1**-**5** (Fig. 1) by combining theoretical and experimental methods. Our key experimental findings are that substitution pattern on the anthracene moiety affects ESIPT reactivity, and that tautomers formed by ESIPT are not emissive. *Ab initio* calculations fully disclosed the mechanistic aspects for the differences in observed photophysics and ESIPT reactivity of **1**-**5**.

Results

Conformational equilibria and singlet excited states for carbaldehydes 1-3

To fully understand the photophysical properties of anthrol carbaldehydes, *ab initio* calculations were performed on molecules **1**-**3**. With respect to the mutual orientation of the hydroxyl and the carbonyl groups, we distinguish between *syn-syn* (A), *syn-anti* (B), *anti-syn* (C) and *anti-anti* (D) conformers (Fig. 2 and Fig. S1 in the ESI). The relative energies of the four conformers were calculated at the MP2/aug-cc-pVDZ level of theory (Table 1). For all three carbaldehydes the *syn-syn* conformers, exhibiting an intra-molecular hydrogen bond, are the most stable structures in gas phase. Computations performed using the COSMO continuum solvation model[48] in acetonitrile confirm that *syn-syn* conformers are the most stable ones.

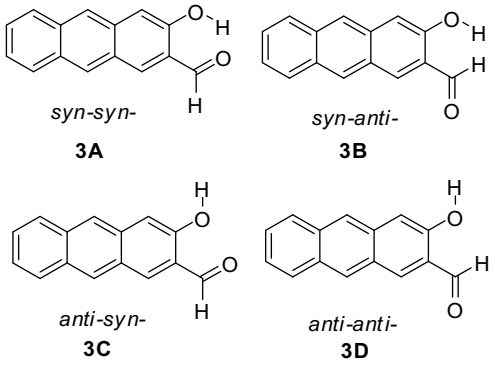

Fig. 2. Conformers of carbaldehyde **3**.

Rotation of the CHOH and OH groups about the C-C and C-O bonds, respectively is strongly destabilizing. In carbaldehyde **3** the *syn-anti* and *anti-syn* structures are found 0.41 (9.45) and 0.38 eV (8.76 kcal/mol) higher in energy. The *anti-anti* structure is weakly stabilized by the O···H interaction, and it is found 0.30 eV (6.91 kcal/mol) above the minimum. From Table 1 it is evident that that the same trend is found for **1** and **2**. Solvation leads to stabilization of the conformers. In particular, in CH_3CN the *anti-anti* structures of **1-3** are found 0.19 (4.38), 0.21 (4.84) and 0.19 eV (4.38 kcal/mol), higher in energy than the corresponding *syn-syn* structures. This ensures that in the ground state the Boltzmann population of conformers B-D is small at room temperature, both in gas phase and in solution, and that these conformers are not the main species in the primary excitation process. However, nonradiative deactivation from the excited electronic states may supply sufficient energy to the system to allow conformational changes. In particular, a relatively low energy barrier of 0.16 eV (3.69 kcal/mol) was found for the conformational change **3B→3D** in S_0 (for the calculated conformational change barriers in S_0 and S_1 see Table S1 in the ESI). Thus, to obtain a wider picture of the reactivity of **1-3**, we explore the excited electronic states properties of all conformers.

The lowest three ADC(2)/aug-cc-pVDZ vertical excitation energies of **1**, **2** and **3** together with the most relevant molecular orbitals involved in the excitation are compiled in Table 2, and Tables S2 and S3 in the ESI. In all carbaldehydes except in **2B**, the lowest excited state (S_1) is a ππ* state with dominant HOMO→LUMO transition, corresponding to the L_a state. While L_a is a locally excited state, it has a partial charge transfer character. This is evident from the frontier orbitals of **3A** shown in Fig. 3, where one sees that translocation of electron density from the anthracene ring to the carbonyl group takes place upon photoexcitation. Higher in energy are the second ππ* state, mostly the L_b state with dominant contribution from HOMO-1→LUMO, and an nπ* state with excitation from the oxygen lone pair orbitals to the anthracene ring. Relevant molecular orbitals contributing to the excitation to S_1, S_2 and S_3 for **3B**-**3D**, as well as for all conformers of **1** and **2** are shown in the supporting information (Figs. S3-S13).

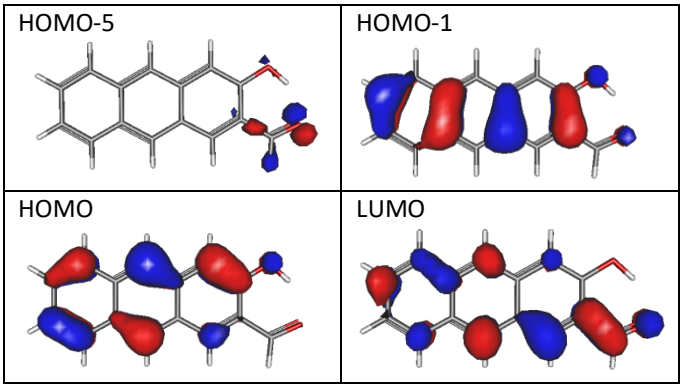

Fig. 3. Relevant molecular orbitals contributing to the S_1, S_2 and S_3 transitions of **3A** computed at the geometry of vertical excitation. The computation were performed at the ADC(2)/aug-cc-pVDZ level.

Journal Name

ARTICLE

Table 1. Relative energies (MP2/aug-cc-pVDZ) of the four conformers of **1**-**3** in the ground electronic state.

	1			**2**			**3**		
	ΔE^{gas} (eV)	ΔE^{ACN} (eV)	ΔE^{EtOAC} (eV	ΔE^{gas} (eV)	ΔE^{ACN} (eV)	ΔE^{EtOAC} (eV)	ΔE^{gas} (eV)	ΔE^{ACN} (eV)	ΔE^{EtOAC} (eV)
A	0.00	0.00	0.00	0.00	0.00	0.00	0.00	0.00	0.00
B	0.41	0.21	0.31	0.57	0.34	0.40	0.41	0.31	0.33
C	0.56	0.28	0.40	0.38	0.29	0.31	0.38	0.20	0.25
D	0.30	0.19	0.30	0.35	0.21	0.25	0.30	0.19	0.21

Table 2. Vertical excitation energies to the three lowest excited states of **3**, oscillator strengths (in parenthesis) and the most relevant molecular orbitals involved in the excitation. The computations were performed at the ADC(2)/aug-cc-pVDZ level.

	3A		**3B**		**3C**		**3D**	
	ΔE (eV)	MO	ΔE (eV)	MO	ΔE (eV)	MO	ΔE (eV)	MO
S_1	2.73 (0.046)	$L_a(\pi\pi^*)$ H→L	2.83 (0.047)	$L_a(\pi\pi^*)$ H→L	3.08 (0.048)	$L_a(\pi\pi^*)$ H→L	3.04 (0.046)	$L_a(\pi\pi^*)$ H→L
S_2	3.64 (0.032)	$L_b(\pi\pi^*)$ H-1→L	3.39 (1×10^{-4})	$n\pi^*$ H-5→L	3.38 (1×10^{-4})	$n\pi^*$ H-5→L	3.38 (1×10^{-4})	$n\pi^*$ H-5→L
S_3	3.67 (2×10^{-4})	$n\pi^*$ H-5→L	3.63 (0.050)	$L_b(\pi\pi^*)$ H-1→L	3.74 (0.023)	$L_b(\pi\pi^*)$ H-1→L	3.69 (0.047)	$L_b(\pi\pi^*)$ H-1→L

Absorption and fluorescence properties of carbaldehydes 1-3

The calculations above are relevant to the measured absorption spectra. Absorption and fluorescence spectra for **1**-**5** were measured in CH_3CN (for all absorption and fluorescence spectra see Figs. S14-S31 in the ESI). In addition, for **1** and **2** the spectra were measured in cyclohexane, and for **3** in cyclohexane and ethyl acetate. Generally, all compounds have the lowest energy absorption band in the visible region (375-550 nm) corresponding to the $S_0 \rightarrow S_1$ transition, populating S_1 state that has the L_a character (Fig. 4). Higher in energy, at ≈ 350 nm, is the absorption band with the typical anthracene vibronic progression, corresponding to the population of the S_2 state that has the L_b character. As demonstrated for **3** (Fig. S22 in the ESI), the lowest absorption band is solvatochromic, exhibiting ≈10 nm hyposchromic shift upon an increase of the solvent polarity from cyclohexane to CH_3CN. The hyposchromic shift indicates that polar solvent stabilizes more S_0 than the Franck Condon (FC) state. The absorption band that corresponds to S_2 is not solvatochromic.

We will see shortly that the conformer dependent energy ordering influences the emission from the lowest excited state of **1-3**. Geometry optimization of the $L_a(\pi\pi^*)$ state provides basic information on emissive properties of these molecules, as well as their ESIPT reactivity. Adiabatic excitation energies (ΔE^a) computed as the energy difference between the optimized ground (S_0^{min}) and excited state structures (S_1^{min}), and vertical emission energies ($E^{emission}$) computed as the difference in energy between the excited and ground state at the S_1^{min} geometry for carbaldehyde **3** are compiled in Table 3 (for **1** and **2** in Tables S4 and S5 in the ESI).

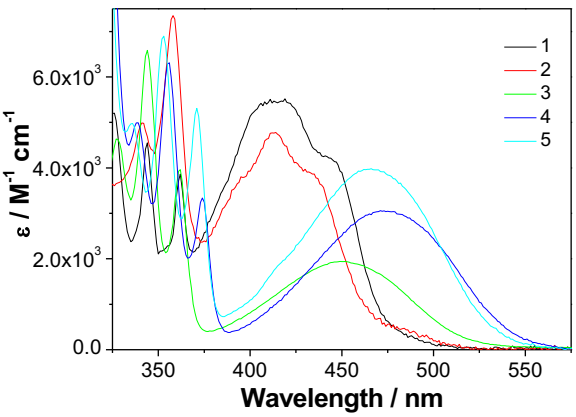

Fig. 4. Absorption spectra of **1**-**5** in CH_3CN.

Table 3. Adiabatic excitation energies (ΔE^a) and vertical emission energies ($E^{emission}$) of **3**. The emission from the bright L_a state is marked in bold.

	3A	3B	3C	3D
ΔE^a (eV)	None (S_1/S_0 CI)	2.58	2.59	2.78
$E^{emission}$ (eV)	None (S_1/S_0 CI)	**2.29**	1.30	**2.49**

Steady-state and time-resolved fluorescence measurements for all molecules were performed in CH_3CN and cyclohexane, but for **3**-**5** fluorescence in cyclohexane could not be detected. For **3**, the fluorescence was also measured in EtOAc (all spectral properties are compiled in Table S5). Fluorescence spectra in CH_3CN are shown in Fig. 5 (for other spectra see Figs. S14-S31 in the ESI). All fluorescence spectra in all investigated solvents are characterized by the presence of one band. In CH_3CN, the emission maxima are at 500-550 nm (in cyclohexane for **1** and **2** at 480 nm). Based on calculations (Table 3, and Tables S4 and S5 in the ESI), the band observed in the fluorescence spectra can be assigned to the locally excited S_1 state. Fluorescence spectra are more solvatochromic then absorption spectra with opposite trends being observed. Upon polarity increase, spectra are bathochromically shifted (for **1** and **2**, ≈20 nm from cyclohexane to CH_3CN), in accord with a partial charge transfer character of S_1 that is more stabilized in polar solvents. Addition of protic solvent significantly quenches fluorescence (see Figs S25 in the ESI) requiring measurements to be conducted in aprotic solvents only. Comparison of the calculated and measured fluorescence maxima is given in Table S7. For **1** and **2** the calculated excitation energies are somewhat overestimated (corresponding to the shift in the absorption spectrum of ≈20 nm), whereas a better correlation was obtained for the emission energies. For compound **3**, a difference between the calculated and experimental values is smaller. Nevertheless,

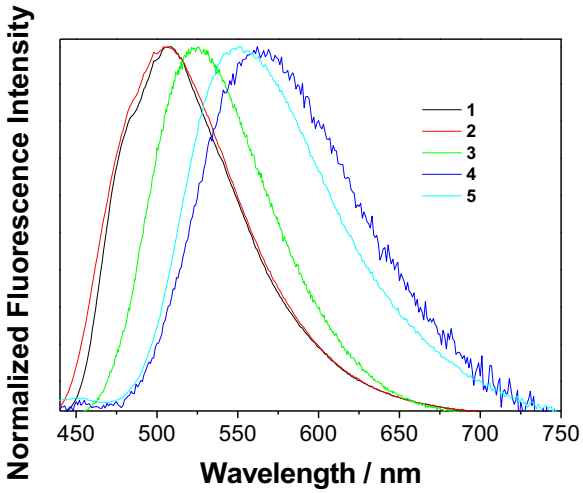

Fig. 5. Normalized fluorescence spectra of **1**-**5** in CH_3CN (λ_{ex} = 420 nm).

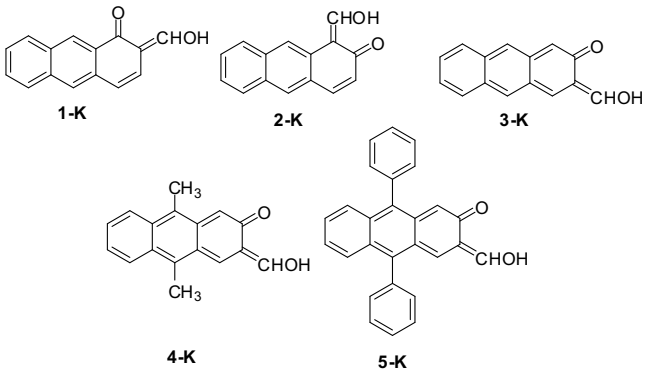

Fig. 6. Anticipated phototautomers from **1**-**5**.

the fluorescence from the phototautomers **1-K**-**5-K** (Fig. 6) formed by ESIPT, or the characteristic dual emission usually seen with the systems undergoing ESIPT were not observed.

Quantum yields of fluorescence were determined by use of acridine yellow as a reference (Φ_F=0.57)[49] whereas decay times from S_1 were measured by time-correlated single photon counting (SPC, Table 4 and Table S8 in the ESI). Fluorescence quantum yields (Φ_F) for **1** and **2** are significantly higher than for **3**-**5**, due to emission from the most stable and the most abundant conformer **1A** or **2A**, from the S_1 surface minimum. On the contrary, the most abundant conformer **3A** is not emissive since it undergoes barrierless ESIPT (*vide infra*), and along the ESIPT pathway deactivates *via* a conical intersection between the S_1 and S_0. Thus, emission for **3** is most probably observed from conformers **3B** or **3D** which are higher in energy (see above) and likely present in small amounts in solution at room temperature.

We notice that in S_0 conformers **3B** and **3D** are 0.31 (7.14 kcal/mol) and 0.19 eV (4.38 kcal/mol) higher in energy then **3A** (Table 1). However, in S_1 the energy ordering of conformers changes, so that **3B** is 0.20 eV more stable than **3D**, although both are higher in energy than **3A**. The barrier for conformational change **3B**→**3D** in S_0 is 0.16 eV (3.69 kcal/mol) and it increases to 0.27 eV (6.22 kcal/mol) in the S_1 state (see Fig. S2 in the ESI). Thus, conformational switch **3B**→**3D** may take place in S_0 if the system acquires enough energy at higher temperature, but in S_1 it is very unlikely since the barrier is relatively high and the excited state has a finite lifetime. On the other hand, the energy barrier for **3D**→**3B** is only 0.09 eV (2.07 kcal/mol) in S_1, allowing for this conformational change during the S_1 lifetime. Thus it is plausible that upon excitation of **3D** (the second conformer in energy in S_0), the switch **3D**→**3B** takes place in S_1. The same behavior is anticipated for **4** and **5**.

For carbaldehydes **3**-**5** the Φ_F depends on the excitation wavelength, whereas the appearance of the excitation spectra depends on the detection wavelength (see Fig S22 in the ESI). Since we excluded the presence of impurities in the sample (for the synthesis see the ESI), the finding suggested that conformers A-D have different absorption spectra. Moreover,

Journal Name

ARTICLE

Table 4. Photophysical properties of **1**-**5**.

	Φ_F (cyclohex. or EtOAc) [a]	τ (cyclohex. or EtOAc) /ns [b]	Φ_F (CH_3CN, 20 °C) [a]	Φ_{20}/Φ_{55} [c]	τ (CH_3CN, 20 °C) /ns[b]	τ (CH_3CN, 54 °C) /ns[b]
1	0.15±0.01[d]	0.1-0.3 3.8 ±0.1 [d]	0.11 ± 0.01	1.43	3.9 ± 0.1	3.4 ± 0.1
2	0.13±0.02[d]	0.1-0.3 3.1 ±0.1 [d]	0.20±0.04	1.80	7.0 ± 0.1	5.8 ± 0.1
3	(400 nm) 0.043 (420 nm) 0.019 (440 nm) 0.013[e,f]	3.1±0.1 27.0±0.1 [f]	(400 nm) 0.017 (420 nm) 0.0092 (440 nm) 0.0069[e]	0.79	23.8 ± 0.1	27.6 ± 0.1
4			(420 nm) 0.0087 (450 nm) 0.0057[e]	0.88	11.8 ± 0.1 20.6 ± 0.1	≈10 ps 3.7 ± 0.5 16.7 ± 0.1
5			(420 nm) 0.043 (450 nm) 0.030[e]	0.88	0.3 ± 0.1 22.6 ± 0.1	0.07 ± 0.01 20.7 ± 0.1

[a] Fluorescence quantum yield was measured by use of acridine yellow as a reference (Φ_F =0.57).[49] An average value is reported from single experiment by excitation at three wavelengths. The errors quoted correspond to maximum absolute deviations. [b] Lifetimes measured by SPC. For multiexponential decays pre-exponential factors are given in Table S8 in the ESI. The errors quoted correspond to maximum absolute deviations. [c] Ratio of integrated spectra at different temperatures. [d] Measured in cyclohexane. [e] Single measurement for different λ_{ex}. [f] Measured in EtOAc.

we see a general trend that Φ_F is higher upon excitation at the shorter wavelength where the less abundant conformers B-D have higher absorptivity than the most stable non-fluorescent conformer A (Table 2). Higher Φ_F upon excitation at shorter wavelength may also be correlated with excitation to a higher vibrational level, leading to the conformational change and population of emissive conformers B and D. However, calculated energy barriers for the conformational change in S_1 are larger than in S_0 (Table S2 in the ESI), indicating that all conformational changes except D→B are improbable during the S_1 lifetimes. Taking into account rotational lifetimes observed for methoxyanthracene where interconversion between the rotamers was observed,[50] **3**-**5** seem to have similar photophysical properties since conformational change D→B probably takes place in S_1.

Fluorescence spectra for **1**-**5** were measured at different temperatures. For **1** and **2**, at higher temperatures the fluorescence decreases, but for **3**-**5** the trend is opposite (see Fig. 7 and Figs. S17, S20, S28 and S31 in the ESI). The increase of Φ_F with temperature for **3**-**5** is in accord with the emission being observed from the less populated conformers B-D whose content in the solution increases with temperature. By assuming that the rate constant for fluorescence from the conformers is not temperature dependent, for carbaldehyde **3** the energy barrier for fluorescence was estimated from the Φ_F dependence on temperature by applying Arrhenius equation (Fig 4 bottom and eq. S4 in the supporting information). The slope of 640 ± 40 K^{-1} corresponds to an activation energy of 0.05 eV (1.2±0.1 kcal/mol) which may be related to the calculated barrier for the OH bond rotational in S_1 and conversion **3D**→**3B**. Since the fluorescence quantum yield generally decreases with temperature which was not accounted for in the estimation of E_a, the value may also represent a lower limit for the conversion of conformers in S_0. For example, the calculated barrier for conversion **3B**→**3D** in S_0 is 0.16 eV.

The decay for the fluorescence of **1**-**3** in CH_3CN are single exponential indicating existence of one emissive species in S_1. For **1** and **2** this decay probably corresponds to conformer A, whereas for **3** it is related to the decay from the exited state of conformer B or D. Single exponential decays measured with the SPC set-up used, did not explicitly indicate that ESIPT in CH_3CN takes place. However, Φ_F for **1** and **2** are significantly lower and S_1 lifetimes are shorter than for the parent 2-anthrol (**10**) in CH_3CN (Φ_F = 0.88, τ = 25.3 ns).[51] Faster decays for the fluorescence of the carbaldehydes indicates the nonradiative deactivation from S_1 occurs, which in principle may be due to ESIPT that populates nonfluorescent keto-tautomers, or intersystem crossing (ISC) that populates triplet states. On the contrary, the fluorescent lifetime for **3** in CH_3CN is comparable to the one for 2-anthrol, due to emission taking place from conformer B or D that cannot undergo ESIPT or ISC (*vide infra*). However, **3B** or **3D** are weakly populated, so the Φ_F is low.

Decay of fluorescence for **1** and **2** in cyclohexane and for **3** in EtOAc was best fit to a function corresponding to the sum of

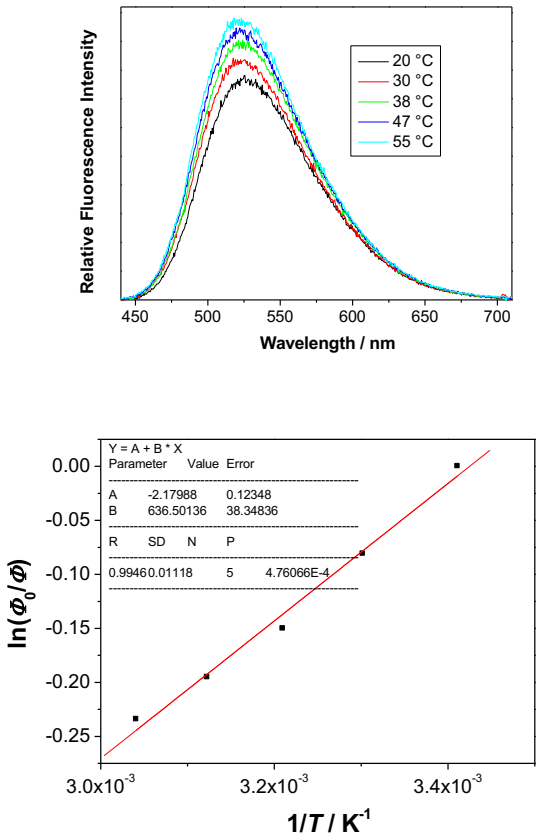

Fig. 7. Fluorescence spectra of **3** in CH_3CN (λ_{ex} = 420 nm) at different temperatures (top) and dependence of the $\ln(\Phi_F/\Phi_F)$ on 1/T (bottom), linear fitting of the data to Arrhenius equation gives the value for the slope of 640±40 K^{-1}.

two exponentials with both pre-exponential factors being positive. If the emission from keto-tautomers was detected, than the emission kinetics collected at long wavelength where only keto-tautomers emit would include a growth component with a negative pre-exponential factor because the keto-tautomers are formed in the S_1 state. The likely reason for the observed dual fluorescence for **1**-**3** in cyclohexane or EtOAc, or for **4** and **5** in CH_3CN is the presence of conformers which have different S_1 lifetimes (see above).

Calculations of ESIPT pathway

ESIPT requires that a translocation of charge from the hydroxyl to the aldehyde group takes place upon electronic excitation. Therefore, the different propensity of **1A**, **2A** and **3A** for ESIPT can be understood from differences in the electron density of the corresponding S_1 and S_0 states shown in Fig 8. Blue regions indicate an increase of electron density in the excited state with respect to the ground state, whereas red areas indicate the reduction of the electron density.

Fig. 8 shows that **1A** and **2A** cannot undergo ESIPT. Moreover, the S_1 potential energy curve along the ESIPT coordinate has a single well corresponding to the reactants, **1A** and **2A** and no evidence for stable keto-tautomers **1-K-A** and **2-K-A** was found. On the other hand, minima have been located on the S_1 surfaces of **1A** and **2A** corresponding to isomers **1-K-B** and **2-K-B** in which rotation about the formally double C=C bond takes place (Fig. 9). However, the energy of these structures is comparable to the energy of the corresponding FC geometries. Specifically, the energy of **1-K-B** is almost isoenergetic with **1A** and the energy of **2-K-B** is 0.25 eV (5.77 kcal/mol) lower than the energy of the **2A** FC geometry. While the solvent can modify these values to some extent we believe that the population of both **1-K-B** and **2-K-B** tautomers is quite unlikely owing to the energy barrier for C=C bond rotation that needs to be surmounted on the way to the formation of photoproducts **1-K-B** and **2-K-B**. However, these tautomers

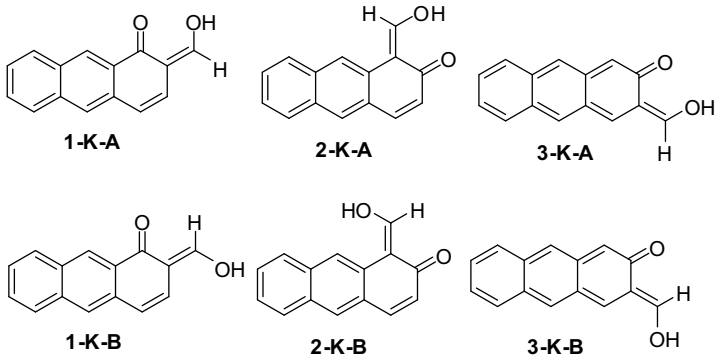

Fig. 9. Anticipated stereoisomers of phototautomers **1-K-3-K**.

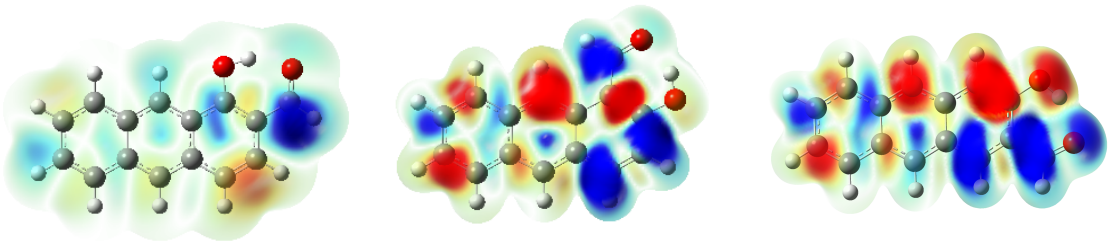

Fig. 8. Projection of the electron density difference between the S_1 and S_0 states on the electron isodensity surface of S_0 at the minimum energy geometry of S_0. **1A** (left), **2A** (middle) and **3A** (right). Areas of depletion (increase) of electron density in the excited states are shown in red (blue).

Journal Name

ARTICLE

may be populated by solvent-assisted ESIPT in protic solvent, accounting for the complete fluorescence quenching.

From Fig. 8 it is evident that a substantial migration of charge from the hydroxyl to the aldehyde group takes place only in **3A**. This sets the stage for ESIPT. Fig. 10 shows the potential-energy profiles of the electronic ground state and of the two lowest excited states, the optically bright $L_a(\pi\pi^*)$ and dark $L_b(\pi\pi^*)$ states, along the proton-transfer reaction path. The driving coordinate is the O–H bond length of the phenolic OH group. The graph describes the movement of the proton from the phenolic OH to the aldehyde group. The potential-energy profile of the L_a state exhibits a shoulder along the proton transfer coordinate, but supports no minimum on the reactant side. The movement of the proton has an opposite effect on the energies of the $L_a(\pi\pi^*)$ and the electronic ground state. While the energy of the $L_a(\pi\pi^*)$ steeply decreases from 3.64 to 1.72 eV, the energy of the ground state increases and the two potential energy surfaces intersect at an O–H distance of ~1.7 Å. Thus, **3A** deactivates non-radiatively to the electronic ground state. Once on the ground electronic state, one would expect that the gradient of the ground state potential energy surface drives the proton back to the phenolic OH group.

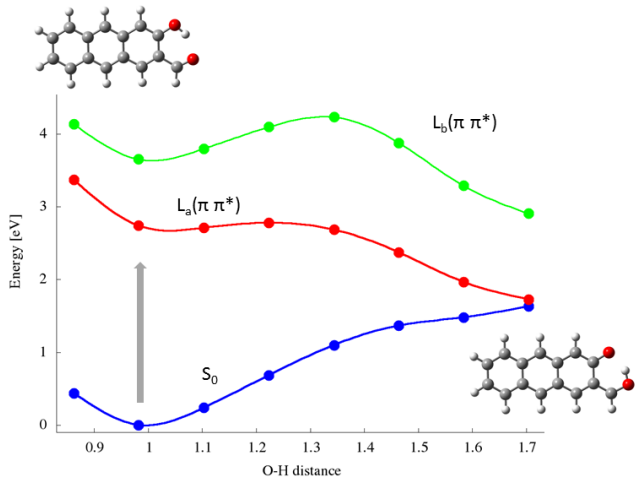

Fig. 10. Energy profiles (in eV) of the electronic ground state (S_0, blue) and the $L_a(\pi\pi^*)$ (red) and $L_b(\pi\pi^*)$ (green) states of **3A**. The energy profiles were obtained by linear interpolation in internal coordinates between the FC and CI geometries. The length of the intramolecular hydrogen bond is given in Å. The insets show the FC and CI geometries (energy profiles including also the two lowest triplet states are shown in Fig S35 and Cartesian coordinates are given in the ESI).

However, the **3-K-A** conformer with rotated H-atom bond has been locate on the ground state surface, 2.05 eV above the global minimum. Due to the large excess in kinetic energy ~ 2 eV (46.12 kcal/mol) that the system has acquired in going from the FC region to the CI, the conformer can be populated. For the rotated conformer the $L_a(\pi\pi^*)$ state is found vertically 1.29 eV (29.73 kcal/mol) higher in energy. In addition, one can consider the **3-K-B** isomer located on the ground state surface 1.89 eV above the global minimum, but the structure is unstable on the $L_a(\pi\pi^*)$ surface and optimization leads to CI with the ground state.

Triplet excited state properties of 1-3

From the above considerations, it is evident that the low Φ_F of **1** and **2** cannot be attributed to ESIPT. Therefore, we considered the possibility that low-lying triplet excited states of the most abundant conformers **1A** and **2A** get populated. Table 5 compiles vertical excitation energies to the lowest two triplet states of **1A**, **2A** and **3D** computed at the S_0^{min} and S_1^{min} geometries, while Figs. S32-S35 in the ESI show the energy profiles of the relevant singlet and triplet excited states in the region from S_0^{min} to S_1^{min}.

Table 5. Vertical excitation energies to the lowest singlet and two lowest triplet excited states computed at S_0^{min} and S_1^{min} geometries for conformers **1A**, **2A** and **3D.** See also Tables S2-S5 and Figures S32-S34 in the ESI.

		Excitation energy (eV)		
Geometry	State	**1A**	**2A**	**3D**
S_0^{min}	T_1	2.18	2.30	2.12
	T_2	3.15	3.09	2.99
	S_1	3.07	3.17	3.04
S_1^{min}	T_1	1.71	1.77	1.61
	T_2	2.81	2.73	3.10
	S_1	2.47	2.47	2.49

Comparing the vertical excitation energies of **1A** to the S_1 and T_2 state one finds an energy difference of -0.08 eV (-1.84 kcal/mol) at S_0^{min} and -0.34 eV (-7.84 kcal/mol) at S_1^{min}. For **2A** (Tables S2 and S4), these values are 0.08 eV (1.84 kcal/mol) at S_0^{min} and -0.26 eV (-5.99 kcal/mol) at S_1^{min}. In both cases the energy gap between the S_1 and T_2 states is relatively small. However, in **1A** the energy gap increases when going from the FC geometry to S_1^{min} while in **2A** the ordering of the S_1 and T_2 states is exchanged meaning that in the region of the

configurational space encompassing the relaxation pathway from FC to S_1^{min} the two states cross. In addition, in the S_1^{min} region where the system is effectively trapped, the S_1-T_2 gap is smaller for **2A** than for **1A**. Therefore, without assuming *a priori* a large difference in the spin-orbit couplings in the two systems, the population of T_2 should be favored in **2A**. Turning to **3D** one finds S_1-T_2 energy gaps of 0.05 eV (1.15 kcal/mol) at the S_0^{min} geometry and -0.61 eV (14.06 kcal/mol) at the S_1^{min} geometry. Here, the larger slope of the S_1 surface points to a fast relaxation from the FC region to the S_1 minimum. Once in the region of the S_1 minimum, the T_2 state is too high in energy to be efficiently populated by ISC. Consequently, considering energies of excited singlet and triplet states, efficient ISC and triplet population are anticipated for **1** and **2**, but not for **3**.

Laser Flash Photolysis (LFP)

LFP was used to detect the keto-tautomers **1K**-**5K**, triplet excited states, or other plausible intermediates in the photochemistry of **1**-**5** (for all transient spectra see Fig. S36-S49 in the ESI). The samples were excited by a YAG laser at 355 nm, or in some cases in the LFP experiments of **3** at 266 nm. The spectra were measured in CH_3CN and CH_3CN-H_2O, where protic solvent was anticipated to affect the ESIPT efficiency. Moreover, the measurements were performed in N_2- and O_2-purged solutions, where O_2 is expected to quench triplet excited states.

In N_2 purged CH_3CN solution of **1**, a transient was detected absorbing over the whole spectrum with maxima at 375 and 485 nm (Fig. S36 and S37 in the ESI). The transient was formed within the laser pulse and it decayed to the baseline with non-exponential kinetics. However, when the laser power was reduced, the decay could be fit to a single exponential function with $k = (6 \pm 2)\times10^4$ s^{-1} ($\tau = 15 \pm 2$ μs). The transient was quenched with O_2 (in O_2-purged CH_3CN $k = 3\times10^7$ s^{-1}, $\tau = 33$ ns), so we assigned this transient to the triplet excited state of **1**. Thus, non-exponential decay kinetics in N_2-purged solution can be attributed to triplet-triplet annihilation. In O_2 purged CH_3CN solution of **1**, at short delay after the laser pulse (40 ns), a negative signal was detected due to fluorescence, whereas at longer delays (60 ns) the triplet is observed, and after its decay no other transient was detected. Addition of H_2O to the O_2-purged CH_3CN did not change the appearance of the transient spectra or decay kinetics of the triplet state of **1**.

Similar to **1**, in the N_2-purged CH_3CN solution of **2** we detected the triplet excited state. It absorbs over the whole spectrum and has maxima at 375 and 525 nm. The triplet is formed within the laser pulse and its signal decays to the baseline with unimolecular kinetics $k = (1.8 \pm 0.1)\times10^5$ s^{-1} ($\tau = 5.5 \pm 0.1$ μs). In O_2-purged solution the triplet is quenched ($k = 2.8\times10^7$ s^{-1}, $\tau =$ 35 ns). In addition to the triplet, in N_2-purged solution, at 300-400 nm we detected a different short-lived transient with the lifetime of $\tau \approx 12$ ns (see Figs. S38 and S39 in the ESI). The transient was tentatively assigned to keto-tautmer **2-K**, although calculations point to inefficient ESIPT. However, due to limits for the time resolution of the LFP set-up, no further experiments were warranted, so unambiguous assignment of the additional transient was not possible.

Transient absorption spectra for **3** are significantly different then for **1** and **2**. In N_2-purged CH_3CN solution in the visible part of the spectrum, at short delays a negative signal due to fluorescence was detected, and at longer delays a positive signal with a maximum at 370 nm (Fig. S40 in the ESI) was observed. Since the maximum of the absorption almost coincides with the excitation wavelength of 355 nm, the sample was excited at 266 nm to get a better quality spectrum (Fig. 11). The transient with the maximum at 370 nm was formed within the laser pulse and its decay was fit to a sum of two exponentials with $k = (3.2\pm0.1)\times10^7 s^{-1}$, ($\tau = 31\pm1$ ns); and $k = (2.7\pm0.1)\times10^6$ s^{-1}, ($\tau = 360\pm10$ ns). In O_2-purged solutions the short-lived transient was not quenched, whereas the long-lived was. Thus, in O_2-purged solution one transient was detected with a maximum of absorption at 370 nm and mono-exponential decay kinetics $k = (3.3\pm0.1)\times10^7 s^{-1}$, ($\tau = 30\pm2$ ns). The short-lived transient was assigned to keto-tautomer **3-K**, whereas the long-lived transient (360 ns) probably corresponds to the triplet excited state of **3**.

To verify the assignment of the transient with a maximum at 370 nm to **3-K**, the LFP measurements were performed for solutions of **3** in CH_3CN-H_2O (1:1) and CH_3CN-D_2O (1:1) which were optically matched at the excitation wavelength (355 nm) under oxygen. Due to a primary isotope effect which should affect the ESIPT kinetics, as well as the kinetics for the decay of keto-tautomer, it was anticipated that in D_2O the transient would be formed with lower initial absorbance right after laser excitation and it would have slower decay kinetics. Surprisingly, we observe a negative isotope effect for the transient formation (judged from the initial absorbance for the transient $k_H/k_D = 0.7$-0.8), whereas the transient decay kinetics is similar in both solvents, $\tau_{D2O} = 91\pm1$ ns, and $\tau_{H2O} = 91\pm5$ ns.

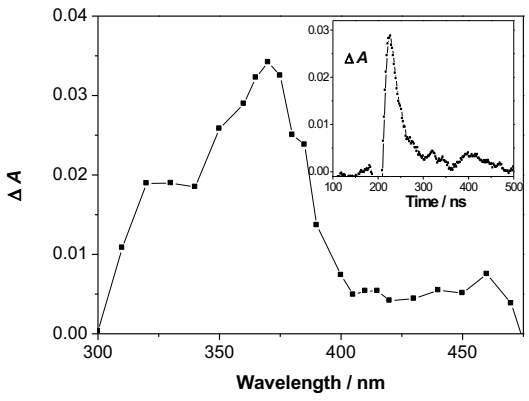

Fig. 11. Transient absorption spectrum of **3** in O_2-purged CH_3CN obtained by exciting at 266 nm with a delay of 40 ns after the laser flash (inset: decay at 380 nm).

Journal Name

ARTICLE

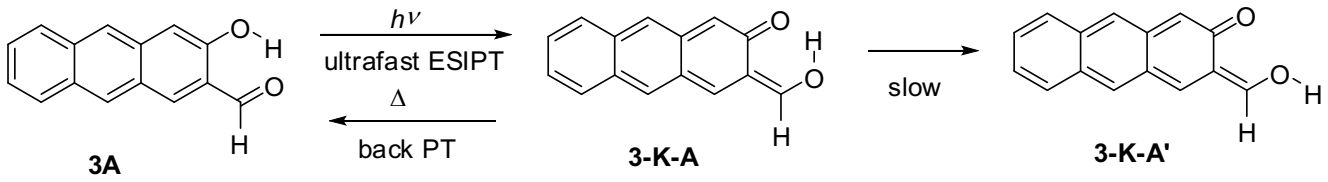

Scheme 1.

Negative isotope effects have been documented for systems where the proton transfer equilibrium is reached first, followed by a slower different rate determining step takes place.[52,53] Consequently, in our system we propose that ESIPT takes place in an ultrafast process (femtosecond timescale) giving ketotautomer **3-K-A**, that rapidly undergoes back proton transfer to **3A**. However, we have probably detected keto-tautomer **3-K-A'** that is formed from high energy tautomer **3-K-A** in a slower process (in picoseconds) not involving proton transfer (Scheme 1). Thus, with the setup used that has a resolution in nanoseconds, only **3-K-A'** was detected, formed within the laser pulse. Transient absorption spectra for **4** and **5** were very similar to those for **3**. In the transient absorption spectra of **4** and **5** in CH_3CN, a transient was detected absorbing at 300-400 nm, whereas in the visible part of the spectrum the negative signal due to the fluorescence dominates. The signal with the maximum at 370 nm for **4** has decays with τ = 20-30 ns, and for **5** τ = 28 ± 1 ns. The decay and the intensity of the transient formation were not affected by O_2, so they were assigned to **4-K** or **5-K**, respectively. In O_2-purged CH_3CN the lifetime of the transient is τ = 28 ± 2 ns (**4-K**), and τ = 38 ± 2 ns (**5-K**). Addition of H_2O affected the transient formation efficiency, they were formed about three times less efficiently, based on the signal intensity at 370 nm, immediately after the laser pulse for the matched absorbances at the excitation wavelength. However, the decay is slower in the aqueous solution with τ = 30-40 ns, and τ = 50 ± 2 ns. In summary, LFP measurements allowed for the detection of triplet states from **1** and **2** and keto-tautomers from **3**-**5**.

Discussion

Photophysical properties and photochemical reactivity of anthrol carbaldehdyes **1**-**3** are significantly different from the behavior known for ESIPT observed with naphthol carbaldehdyes. From the qualitative investigation of frontier molecular orbitals involved in the population of S_1, the above findings for **1**-**3** are at first sight anti-intuitive. For all three derivatives the most stable conformer is the *syn-syn* (conformer A) with an intramolecular H-bond. Furthermore, the LUMO orbital is significantly localized at the C-C bond between the anthracene and the carbonyl, making it partly double bond in character, and the LUMO has an orbital lobe on the carbonyl oxygen, leading to the expectation that the carbonyl should have an increased electron density in S_1 (Fig. 3, and S3 and S7 in the supporting information). The fluorescence solvatochromic properties for **1**-**3** are in agreement with a polarized S_1 state, which is a prerequisite for ESIPT to occur. However, the quantitative investigation for the electron density difference between S_1 and S_0 (Fig. 5) clearly demonstrates that electronic excitation leads to translocation of charge needed for ESIPT in anthrol **3** only, where the electron density in S_1 increases at the carbonyl oxygen. On the contrary, the electron density in S_1 is located on the carbonyl C-atom in **1** and in the anthracene rings in **2**. Hence, **3** undergoes barrierless ESIPT, whereas for **1** and **2** formation of keto-tautomers is not plausible since it would be highly endergonic, and the corresponding **1-K-A** and **2-K-A** do not have minima on the excited state surface. On the other hand, ESIPT has been observed for both 1,2- and 2,3-substituted naphthol carbaldehydes derivatives.[41-44] Thus, 1,2-substituted naphthols derivatives (analogous to **1** and **2**) show emission of phototautomers in aprotic solvents. However, in protic solvents where the intramolecular H-bond between the carbonly group and the phenolic OH is perturbed, the emission of the locally excited state of naphthols was detected,[41,43] whereas **1** and **2** are not emissive. Comparing naphthol and anthrols clearly indicate that additional fused benzene ring affects the electronic distribution in S_1 leading to different photophysical properties and photochemical reactivity.

Due to generally high stabilization of the *syn-syn* conformer A compared to B-D conformers, with larger energy differences between the conformers in S_1 (Table S2), the conformer conversions are not likely to occur during excited state lifetimes, except for **3D**→**3B** for which a low energy barrier of only 0.09 eV was found. For **1**-**3** in CH_3CN, single exponential decays of fluorescence indicate the presence of only one emitting species in S_1. On the other hand, the likely reason for

the observed dual fluorescence for **1**-**3** in cyclohexane and **4**-**5** in CH_3CN with a low contribution of one decay component is probably due to a small contribution from confomers B-D that are populated in S_0. Consequently, photophysical properties and photochemical reactivity of **1**-**3** are mostly governed by the NEER principle (non-equilibration of the excited-state rotamers).[54,55] That is, the conformer distribution in S_0 is mostly maintained upon excitation to S_1 due to improbable conformer interconversions in S_1 imposed by high energy barriers. Since anthrols **1** and **2** are not reactive in ESIPT, their most abundant conformers **1A** and **2A** are emissive. Therefore, Φ_F for **1** and **2** is about ten times higher than for **3**.

Shorter singlet lifetimes for **1** and **2** compared to **3** and 2-anthrol are due to nonradiative decay from S_1 by ISC. Assuming that difference in singlet lifetimes for **2** and 2-anthrol is only due to ISC, the rate constant for ISC in **2** can be approximated, $k_{ISC} \approx 1\times10^8$ s^{-1}. This rate represents only an upper limit since ISC is in competition with internal conversion (IC). The obvious reason for the efficient ISC in anthracene derivatives **1** and **2** is the existence of the triplet T_2 state with energy that is comparable to the FC or relaxed S_1 state energies (Table 5). For the analogous naphthols, the energy differences between the singlet and triplet excited states are larger, and ISC takes place only in the non-hydrogen bonded conformers in protic solvents,[41] where the ESIPT does not compete with ISC.

Although anthrol **3** reacts in ESIPT, it does not exhibit the typical dual fluorescence, as is the case with salicylaldehyde or naphthol carbaldehyde derivatives. Namely, along the ESIPT trajectory, a conical intersection with the S_0 leads to the formation of **3-K** tautomer in the hot ground state followed by non-radiative deactivation of the S_1 of **3** to the ground state. In this sequence conformer A is repopulated, but the amount of energy supplied by the IC (1.73 eV) may lead to conformational changes. The fluorescence is detected only from the locally excited state of non-reactive, less populated conformers **3B** or **3D**. Consequently, Φ_F increases with temperature and depends on the excitation wavelength. This finding is unprecedented to the ubiquitous molecules undergoing ESIPT where the characteristic Stokes-shifted emission was observed.[38-44]

Keto-tautomer **3-K** was detected by LFP. The negative isotope effect for the formation of the detected transient indicated that this transient corresponded to conformer **3-K-A'** whose formation may be possible from the hot-ground state of **3-K-A** reached *via* a S_1/S_0 conical intersection, or to stereoisomer **3-K-B** populated by H_2O-assisted formal ESIPT. In analogy, the keto-tautomers detected by LFP from structurally similar molecules **4** and **5** probably correspond to the analogous structures **4-K-A'** and **5-K-A'**. Population of these keto-tautomers that have longer lifetimes then the usual emissive keto-tautomers formed by ESIPT may find applications in different aspects of material science or in organic synthesis if some suitable quenchers could be found that would react with **3-K** to **5-K** in a Diels-Alder reaction giving complex molecular structures. Formation of keto-tautomer **3-K** from **3-A** is in principle possible also on the triplet excited state surface (see Fig S35 in the ESI). However, it can be accomplished only by use of a triplet sensitizer that would excited **3A** to the triplet state. Direct excitation of **3A** leads to deactivation via ESIPT so that the triplet state can never be reached.

Although tautomers formed by ESIPT from anthrol carbaldehydes are not emissive, photochemically reactive anthrols may have numerous applications, primarily due to the fact that they can be excited by visible light. Thus, applicability of these molecules as photoswitches, photostabilizers, temperature or H_2O sensors in material science as well as in biology is anticipated.

Conclusions

Photophysical properties and photochemical ESIPT reactivity of anthrol carbaldehydes **1**-**5**, compared to the corresponding naphthol carbaldehydes, is unexpected and unprecedented. Surprisingly, 1,2-disubstituted anthrol carbaldehydes **1** and **2** are not ESIPT reactive, whereas 2,3-disubstituted anthrols **3**-**5** undergo efficient barrierless ultrafast ESIPT. However, unlike the usual molecules undergoing ESIPT, the typical dual emission from locally excited states and ESIPT tautomers were not observed since ESIPT proceeds *via* a conical intersection with S_0 delivering keto-tautomer in the hot ground state. It is an important finding, which calls in question some literature precedent where ESIPT was reported not to take place due to the lack of tautomer emission. Consequently, findings described herein have significant impact in understanding ESIPT reactivity in general. We fully disclosed reasons that lead to different photophysical properties and reactivity of naphthol and anthrol carbaldehydes. The fact that a small change of chromophore by addition of one benzene ring has profound consequences should be taken into account when designing molecules for different applications.

Experimental and computational methods

Steady-State and Time-Resolved Fluorescence Measurements

Stock solutions of **1**-**5** were prepared by dissolving 2-3 mg of the compound in 10 mL CH_3CN (corresponding to concentrations of 6.0×10^{-4}-1.3×10^{-3} M) For the absorption and fluorescence measurements, the stock solutions were diluted 20-100 times so the final concentrations in CH_3CN were 1×10^{-5}-3×10^{-5} M. Absorption measurements were performed on a Cary 1 spectrometer. Fluorescence measurements were performed on a PTI QM40 fluorometer. All slits (excitation and emission) were set to a bandpass of 2 nm (5 nm in case of **3**-**5**). The spectra were corrected for fluctuations in the lamp intensity and transmission of optics. Fluorescence quantum yields were determined by use of acridine yellow as reference (Φ_F=0.57),[49] which prior to the measurements was recrystallized three times from CH_3OH. Carbaldehydes **1** and **2** were excited at 410, 420 or 430 nm, and the emission was collected in the range 430-800 nm. For carbaldehydes **3**-**5** the excitation was at 400, 420 and 450 nm or 420 and 450 nm and the emission was detected in the range 440-800 nm. Two or three quantum yields were calculated (eq. S2 in the Supporting

Information) and the mean value was reported. The measurements were performed in the temperature range 20-54 °C, and the temperature was maintained by a thermostat which was calibrated.

Fluorescence decays, collected over 1023 time channels, were obtained on an Edinburgh Instruments OB920 single photon counter using a light emitting diode for excitation at 405 nm. The instrument response function (IRF), using LUDOX as the scatterer, were recorded at the same wavelength as the excitation wavelength and had the half width of the IRF was ≈ 0.2 ns. The time increment per channel was 0.098 ns for **1** and **2**, or 0.049 ns for **3-5**. Emission decays for samples were recorded until they reached 3×10^3 counts in the peak channel at 500 and 530 nm for **1** and **2**, and at 550 and 575 nm for **3** - **5**. Global analysis of two or three decays was performed by fitting to the decay to sums of exponentials using global Gaussian-weighted non-linear least-squares fitting based on Marquardt-Levenberg minimization implemented in the Fast software package from Edinburgh Instruments. In the global analysis, the decay times were linked for the traces collected at different wavelengths. The fitting parameters (decay times and pre-exponential factors, eq. S1 in the supporting information) were determined by minimizing the reduced chi-square χ^2 and graphical methods were used to judge the quality of the fit that included plots of the weighted residuals *vs*. channel number.

Laser Flash Photolysis (LFP)

All LFP studies were performed on a system previously described[56] using as an excitation source a pulsed Nd:YAG laser at 355 or 266 nm (<20 mJ per pulse), with a pulse width of 10 ns. Static cells (7 mm×7 mm) were used and the solutions were purged with nitrogen or oxygen for 20 min prior to performing the measurements. Absorbances at 355 or 266 nm were ~ 0.3-0.5.

Calculations

The ground state geometries of four possible conformers of carbaldehydes **1**-**3** were optimized using the MP2 method with the resolution of identity approximation (RI).[57] The Dunning correlation consistent basis set augmented with polarization and diffuse functions, aug-cc-pVDZ, was used throughout the work.[58] The relative energies of the conformers were determined in the gas phase. To investigate the effect of the solvent on the energy ordering a continuum solvation model, the conductor-like screening model (COSMO) was used.[55] For the simulation of bulk acetonitrile (CH_3CN) and ethyl acetate (EtOAC) environments we chose dielectric constant of ε = 37.5 and ε = 6.0, respectively. All calculations were performed with Turbomole 7.0.[57]

The algebraic diagrammatic construction to second order (ADC(2)) method was selected to investigate excited electronic states.[59,60] The method is suitable for investigating low lying ππ* states in fused aromatic ring systems as the ordering of the $L_a(\pi\pi^*)$ or $L_b(\pi\pi^*)$ states and the interstate gap are typically well described with ADC(2).[61,62] Adiabatic excitation energies were computed by optimizing both ground and excited state structures.

Conflicts of interest

There are no conflicts to declare.

Acknowledgements

These materials are based on work financed by the Croatian Science Foundation (HRZZ, IP-2014-09-6312 and IP-2016-06-1142), the Unity through Knowledge Fund (UKF-B1) and the Natural Sciences and Engineering Research Council of Canada for (NSERC - RGPIN-121389-2012). NB thanks Professor P. Wan for the financial support and use of laboratory facilities during the visit to UVic.

Notes and references

1 J. F. Ireland, P. A. H. Wyatt, *Adv. Phys. Org. Chem.*, 1976, **12**, 131-221.
2 L. G. Arnaut, S. J. Formosinho, *J. Photochem. Photobiol. A: Chem.*, 1993, **75**, 1-20.
3 W. Klöpffer, *Adv. Photochem.*, 1977, **10**, 311-358.
4 S. J. Formosinho, L. G. Arnaut, *J. Photochem. Photobiol. A: Chem.*, 1993, **75**, 21-48.
5 *Hydrogen-transfer reactions*, ed. J. T. Hynes, J. P. Klinman, H.-H. Limbach, R. L. Schowen, Wiley-VCH, Weinheim, 2007.
6 J. I. Kwon, S. Y. Park, *Adv. Mater*., 2011, **23**, 3615-3642.
7 V. S. Padalkar, S. Seki, *Chem. Soc. Rev*., 2016, **45**, 169-202.
8 K. Choi, A. D. Hamilton, *Angew. Chem. Int. Ed*., 2001, **40**, 3912-3915.
9 A. S. Klymchenko, A. P. Demchenko, *J. Am. Chem. Soc*., 2002, **124**, 12372-12379.
10 X. Peng, Y. Wu, J. Fan, M. Tian, K. Han, *J. Org. Chem*., 2005, **70**, 10524-10531.
11 R. M. F. Batista, E. Oliveira, S. P. G. Costa, C. Lodeiro, M. M. M. Raposo, *Org. Lett*., 2007, **9**, 3201-3204.
12 J. Zhao, S. Ji, Y. Chen, H. Guo, P. Yang, *Phys. Chem. Chem. Phys.*, 2012, **14**, 8803-8817.
13 B. Liu, H. Wang, T. Wang, Y. Bao, F. Du, J. Tian, Q. Li, R. Bai, *Chem. Commun.*, 2012, **48**, 2867-2869.
14 L. V. Schäfer, G. Groenhof, A. R. Klingen, G. L. Ullmann, M. Boggio-Pasqua, M. A. Robb, H. Grubmüller, *Angew. Chem. Int. Ed*., 2007, **46**, 530-536.
15 L. Feng, Z.-M. Liu, J. Hou, X. Lv, J. Ning, G.-B. Ge, J.-N. Cui, L. Yang, *Biosensors and Bioelectronics*, 2015, **65**, 9-15.
16 J. Zhang, L. Ning, J. Liu, J. Wang, B. Yu, X. Liu, X. Yao, Z. Zhang, H. Zhang, *Anal. Chem.* 2015, **87**, 9101-9107.
17 O. F. Mohammed, D. Pines, E. T. J. Nibbering, E. Pines, *Angew.Chem. Int .Ed.*, 2007, **46**, 1458-1461.
18 D. A. Parthenopoulos, D. P. McMorrow, M. Kasha, *J. Phys. Chem.*, 1991, **95**, 2668-2674.
19 J. Catalan, J. C. del Valle, *J. Am. Chem. Soc.*, 1993, **115**, 4321-4325.
20 G. J. Stueber, M. Kieninger, H. Schettler, W. Busch, B. Goeller, J. Franke, H. E. A. Kramer, H. Hoier, S. Henkel, P. Fischer, H. Port, T. Hirsch, G. Rytz, J.-L. Birbaum, *J. Phys. Chem.*, 1995, **99**, 10097-10109.
21 J. Keck, H. E. A. Kramer, H. Port, T. Hirsch, P. Fischer, G. Rytz, *J. Phys.Chem.*, 1996, **100**, 14468-14475.
22 A. L. Sobolewski, W. Domcke, *Phys. Chem. Chem. Phys.*, 2006, **8**, 3410-3417.

23 P. Chou, D. McMorrow, T. J. Aartsma, M. Kasha, *J. Phys. Chem.*, 1984, **88**, 4596-4599.
24 P.-T. Chou, M. L. Martinez, J. H. Clements, *Chem. Phys. Lett.*, 1993, **204**, 395-399.
25 A. Douhal, F. Amat-Guerri, A. U. Acuňa, K. Yoshihara, *Chem. Phys. Lett.*, 1994, **217**, 619-625.
26 S. Park, O.-H. Kwon, S. Kim, S. Park, M.-G. Choi, M. Cha, S. Y. Park, D.-J. Jang, *J. Am. Chem. Soc.*, 2005, **127**, 10070-10074.
27 S. Park, O.-H. Kwon, Y.-S. Lee, D.-J. Jang, S. Y. Park, *J. Phys. Chem. A*, 2007, **111**, 9649-9653.
28 S. Park, J. E. Kwon, S. H. Kim, J. Seo, K. Chung, S.-Y. Park, D.-J. Jang, B. M. Medina, J. Gierschner, S. Y. Park, *J. Am. Chem. Soc.*, 2009, **131**, 14043-14049.
29 K.-C. Tang, M.-J. Chang, T.-Y. Lin, H.-A. Pan, T.-C. Fang, K.-Y. Chen, W.-Y. Hung, Y.-H. Hsu, P.-T. Chou, *J. Am. Chem. Soc.*, 2011, **133**, 17738-17745.
30 R. M. D. Nunes, M. Pineiro, L. G. Arnaut, *J. Am. Chem. Soc.*, 2009, **131**, 9456-9462.
31 S.-J. Lim, J. Seo, S. Y. Park, *J. Am. Chem. Soc*. 2006, **128**, 14542-14547.
32 M. F. Rode, A. L. Sobolewski, *J. Phys. Chem. A*, 2010, **114**, 11879-11889.
33 T. Mutai, H. Tomoda, T. Ohkawa, Y. Yabe, K. Araki, *Angew. Chem. Int. Ed.*, 2008, **47**, 9522-9524.
34 M. Lukeman, P. Wan, In *CRC Handbook of Organic Photochemistry and Photobiology*, ed. W. Horspool, F. Lenci, CRC Press, Boca Raton, 2004., p **39**-1-**39**-19.
35 D. Le Gourrierec, S. M. Ormson, R. G. Brown, *Prog. React. Kinet.*, 1994, **19**, 211-275.
36 S. M. Ormson, R. G. Brown, *Prog. React. Kinet.*, 1994, **19**, 45-91.
37 A. Weller, *Z. Elelctrochem.*, 1956, **60**, 1144-1147.
38 S.-I. Nagaoka, N. Hirota, M. Sumitani, K. Yoshihara, *J. Am. Chem. Soc*. 1983, **105**, 4220-4226.
39 S.-I. Nagaoka, U. Nagashima, *Chem. Phys.*, 1989, **136**, 153-163.
40 A. Migani, L. Blancafort, M. A. Robb, A. D. DeBellis, *J. Am. Chem. Soc.*, 2008, **130**, 6932-6933.
41 P. Chowdhury, S. Panja, S. Chakravorti, *J. Phys. Chem. A*, 2003, **107**, 83-90.
42 S. Mahanta, R. B. Singh, S. Kar, N. Guchait, *Chem. Phys.* 2006, **324**, 742-752.
43 R. B. Singh, S. Mahanta, S. Kar, N. Guchait, *Chem. Phys.* 2007, **331**, 373-384.
44 K. C. Wu, Y.-M. Cheng, Y.-S. Lin, Y.-S. Yeh, S.-C. Pu, Y.-H. Hu, J.-K. Yu, P.-T. Che, *Chem. Phys. Lett.*, 2004, **384**, 203-209.
45 C. Bohne, S. R. Kennedy, R. Boch, F. Negri, G. Orlandi, W. Siebrand, J. C. Scaiano, *J. Phys. Chem.*, 1991, **95**, 10300-10306.
46 Đ. Škalamera, J. Veljković, L. Ptiček, M. Sambol, K. Mlinarić-Majerski, N. Basarić, *Tetrahedron*, 2017, **73**, 5892-5899.
47 Đ. Škalamera, K. Mlinarić-Majerski, I. Martin Kleiner, M. Kralj, J. Oake, P. Wan, C. Bohne, N. Basarić, *J. Org. Chem.*, 2017, **82**, 6006-6021.
48 T. H. Dunning Jr, *J. Chem. Phys.*, 1989, **90**, 1007-1023.
49 J. Olmsted, III, *J. Phys. Chem.*, 1979, **83**, 2581-2584.
50 M. Albrecht, C. Bohne, A. Graznhan, H. Ihmels, T. C. S. Pace, A. Schnurpfeil, M. Waidelich, C. Yihwa, *J. Phys. Chem. A*, 2007, **111**, 1036-1044.
51 Đ. Škalamera, K. Mlinarić-Majerski, I. Martin-Kleiner, M. Kralj, P. Wan, N. Basarić, *J. Org. Chem.*, 2014, **79**, 4390-4397.
52 Y. Chiang, A. J. Kresge, Y. Zhu, *J. Am. Chem. Soc.*, 2001, **123**, 8089-8094.
53 Y. Chiang, A. J. Kresge, Y. Zhu, *J. Am. Chem. Soc.*, 2002, **124**, 717-722.
54 Jacobs, H.J.; Havinga, E., *Adv. Photochem.*, 1979, **11**, 305-373.
55 U. Mazzucato, F. Momicchioli, *Chem. Rev.*, 1991, **91**, 1679-1719.
56 Y. Liao, C. Bohne, *J. Phys. Chem.*, 1996, **100**, 734-743.
57 F. Weigend, M. Häser, *Theor. Chem. Acc.*, 1997, **97**, 331-340.
58 F. Furche, R. Ahlrichs, C. Hättig, W. Klopper, M. Sierka, F. Weigend, *Wiley Interdiscip. Rev. Comput. Mol. Sci.* 2014, **4**, 91-100.
59 A. B. Trofimov, J. Schirmer, *J. Phys. B At. Mol. Opt. Phys.*, 1995, **28**, 2299-2324.
60 A. Dreuw, M. Wormit, *Wiley Interdiscip. Rev. Comput. Mol. Sci.*, 2015, **5**, 82-95.
61 A. Prlj, M. E. Sandoval-Salinas, D. Casanova, D. Jacquemin, C. Corminboeuf, *J. Chem. Theory Comput.*, 2016, **12**, 2652–2660.
62 J. Novak, A. Prlj, N. Basarić, C. Corminboeuf, N. Došlić, *Chem. Eur. J.*, 2017, **23**, 8244-8251.

